Analysis of limited-diffractive and limited-dispersive X-waves generated by finite radial waveguides

Walter Fuscaldo, Santi C. Pavone, Guido Valerio, Alessandro Galli, Matteo Albani, Mauro Ettorre

Analysis of limited-diffractive and limited-dispersive X-waves generated by finite radial waveguides

Walter Fuscaldo,[1,2] Santi C. Pavone,[3] Guido Valerio,[4] Alessandro Galli,[1] Matteo Albani,[3] and Mauro Ettorre[2]

[1] *Dipartimento di Ingegneria dell'Informazione, Elettronica e Telecomunicazioni, Università degli Studi di Roma Sapienza, Via Eudossiana 18, 00184 Roma, Italy.*[*]

[2] *Institut d'Électronique et de Télécommunications de Rennes (IETR), UMR CNRS 6164, Université de Rennes 1, 35042 Rennes, France.*[†]

[3] *Dipartimento di Ingegneria dell'Informazione e Scienze Matematiche, Università degli Studi di Siena, via Roma 56, 53100, Siena, Italy.*

[4] *Sorbonne Université, Université Pierre et Marie Curie, Laboratoire d'Électronique et Électromagnétisme, 75252 Paris, France*

(Dated: April 26, 2016)

In this work we analyze the spatial and temporal features of electromagnetic X-waves propagating in free space and generated by planar radiating apertures. The performance of ideal X-waves are discussed and compared to practical cases where the important effects related to the finiteness of the radiating aperture and the wavenumber dispersion are taken into account. In particular, a practical device consisting of a radial waveguide loaded with radiating slots aligned along a spiral path is considered for the practical case in the millimeter-wave range. A common mathematical framework is defined for a precise comparison of the spatiotemporal properties and focusing capabilities of the generated X-wave. It is clearly shown that the fractional bandwidth of the radiating aperture has a key role in the longitudinal confinement of an X-wave in both ideal and practical cases. In addition, the finiteness of the radiating aperture as well as the wavenumber dispersion clearly affect both the transverse and the longitudinal profile of the generated radiation as it travels beyond the depth-of-field of the generated X-wave. Nevertheless, the spatiotemporal properties of the X-wave are preserved even in this 'dispersive-finite' case within a defined region and duration related to the nondiffractive range and fractional bandwidth of the spectral components of the generated X-wave. The proposed analysis may open new perspectives for the efficient generation of X-waves over finite radiating apertures at millimeter waves where the dispersive behavior of realistic devices is no longer negligible.

PACS numbers: 41.20.Jb, 42.25.Fx, 42.60.Jf, 84.40.Ba, 89.20.Kk

I. INTRODUCTION

In the last decades the generation of localized electromagnetic waves has gained a growing interest among different research communities. Nondiffracting waves [1] (or localized waves [2] as well) are exact solutions to the wave equation that do not exhibit either time or spatial broadening as they propagate. Nevertheless, although spatial and temporal confinements of an electromagnetic wave are closely related to each other, nondiffractive beams (monochromatic solutions) and pulses (polychromatic solutions) have been developed almost independently.

The earlier works on nondiffractive beams, and in particular on Bessel beams [3, 4], paved the way for the realization of optical devices [5] able to generate a nondiffractive intensity profile over a considerable depth of field. In optics, as well as at lower frequencies, different methods have been proposed for generating Bessel beams [6–17] (for a review, see, e.g., [18, 19]). The works at millimeter waves [11–16] are of particular interest since they avoid the ray-optics approximation used at optical frequencies, which limits the analysis of Bessel beams to those with a spot size much larger than the operating wavelength [20].

Nondispersive electromagnetic pulses were discovered during the 80's, mainly thanks to the seminal work on Focus Wave Modes (FWM) [21]. As for ideal Bessel beams, these solutions were endowed by infinite energy [22, 23], and thus nonphysical. (However, exact finite-energy solutions of Maxwell's equations in vacuum have been derived [24].) Nonetheless, a particular class of these nondispersive, nondiffracting solutions, known as X-waves [25], has been studied in different branches of physics, especially in acoustics [26] and optics [27], where X-waves have been generated using finite apertures.

Despite the large amount of works on X-waves (see [1] and Refs. therein), most of them study the generation of X-waves under specific hypotheses, not always verified at millimeter waves. In particular, X-waves are frequently assumed to be superluminal [28], nondispersive [29], and generated by infinite radiating apertures [22]. As a matter of fact, the generation of X-waves from finite apertures has been addressed in several works [25, 29–36], but only few of them [32, 33] have taken into account both the finiteness of the aperture and the wavenumber dispersion with frequency. Therefore, there is still a lack of a comprehensive study providing a detailed and suitable description of the focusing properties of such X-waves.

[*] fuscaldo@diet.uniroma1.it

[†] mauro.ettorre@univ-rennes1.fr

In most practical applications, especially at millimeter waves [11–16], the radiating aperture is finite and the wavenumber varies nonlinearly with frequency. Neglecting dispersion in such polychromatic solutions is thus not possible for an accurate analysis.

In this work we aim to provide an analytical description of *band-limited*, *dispersive*, electromagnetic X-waves generated by *finite apertures* analyzing such effects at millimeter wavelengths. It is worth mentioning that an attempt to generate X-waves at microwaves is provided in [37]. However, other explanations of the observed superluminal propagation are given in literature [34]. Unfortunately, no results have been provided regarding their focusing capabilities. Moreover, to the authors' best knowledge the possibility to generate nondiffracting waves over a considerable fractional bandwidth by means of a realistic millimeter-wave device has never been analyzed in details.

To this aim, our discussion starts from the original formulation of an ideal X-wave. We then show how, by progressively removing all the simplifying hypotheses, it is still possible to generate an electromagnetic pulse with very interesting limited-diffraction and limited-dispersion properties. In particular, we first take into account the dispersion features of an X-wave, assuming a second-order Taylor expansion of the relevant wavenumbers. Then, the intensity profiles along the longitudinal and the transverse axes are calculated in closed-form and compared with those of an ideal X-wave. Finally, we consider a practical case in which a centrally-fed radial waveguide loaded with radiating slots aligned along a spiral path is proposed, in order to generate 'dispersive-finite' X-waves (i.e., X-waves with non-negligible wavenumber dispersion and generated by finite apertures) with very interesting focusing properties. As will be shown, such features result from the peculiar wavenumber dispersion exhibited by the considered radiating aperture.

We demonstrate that a dispersive-finite X-wave (even if it can no longer be considered nondiffractive and nondispersive in the most rigorous sense) retains very interesting localization properties in both transverse and longitudinal profiles over a finite distance and time duration related to the physical size and bandwidth of the generating device. The features may be of interest in various applications at millimeters waves and optics, where the spatial confinement of electromagnetic pulses is of paramount importance and the behaviors of most devices are well defined only in a limited frequency band.

II. SPATIAL CONFINEMENT PROPERTIES OF X-WAVES

The mathematical description of an ideal X-wave (also known as ordinary X-shaped pulse) is given by [1, 2]:

$$\chi(\rho,z,t)=\int_{-\infty}^{+\infty}F(\omega)J_0[k_\rho(\omega)\rho]e^{-jk_z(\omega)z}e^{j\omega t}d\omega \qquad (1)$$

where J_0 is the zeroth-order Bessel function of the first kind, $F(\omega)$ is the frequency spectrum, ω is the angular frequency, z is the axis of propagation, and k_ρ, k_z are the transverse and longitudinal wavenumbers, respectively, related by the separation relation:

$$k^2=k_\rho^2+k_z^2 \qquad (2)$$

with $k=\omega/c$ the free-space wavenumber and c the velocity of light in vacuum. In particular, ideal X-waves can be thought as a superposition of ideal Bessel beams sharing the same *axicon angle* θ:

$$\theta=\arctan(k_\rho/k_z) \qquad (3)$$

and thus, replacing Eqs. (3) and (2) in Eq. (1) yields:

$$\chi(\rho,z,t)=\int_{-\infty}^{+\infty}F(\omega)J_0\left(\frac{\omega}{c}\sin\theta\rho\right)\times\exp\left[-j\frac{\omega}{c}\cos\theta\left(z-\frac{ct}{\cos\theta}\right)\right]d\omega \qquad (4)$$

In such representation, some simplifying hypotheses are tacitly assumed: i) the aperture field is a nondiffractive Bessel beam over the entire frequency range and along an infinite propagating distance. This means that an infinite aperture, or infinite energy is required [3, 4]; ii) the axicon angle θ does not change with frequency. This latter condition implies that no wavenumber dispersion is taken into account.

However, even under these simplifying hypotheses, it is readily shown in the following that is not always possible to efficiently confine a pulse along both the transverse and the longitudinal axis. To this aim, a 'metric' has to be defined in order to intuitively characterize the *spatial confinement efficiency* of the pulse. It is known [4] that a practical realization of X-waves requires a finite radiating aperture of radius ρ_{ap} [25], which limits the nondiffracting behavior of the constituent Bessel beams within a certain 'depth of field' z_{dof} along the z-axis, given by [3]:

$$z_{\mathrm{dof}}=\rho_{\mathrm{ap}}\cot\theta \qquad (5)$$

Therefore, the spatial features of an ideal X-wave are well defined only within a certain ρz-plane limited by ρ_{ap} and z_{dof} along the ρ- and z-axis, respectively. As a consequence, the energy of the pulse is *efficiently* confined along the ρ-axis if and only if the 'spot width' along ρ (S_ρ) is much smaller than the aperture size (ρ_{ap}). Similarly, the confinement along the z-axis is effective if and only if the spot width along z (S_z) is smaller than the depth of field z_{dof}. However, since we are also interested in solutions that are not efficiently confined in one direction but 'extremely' confined along the other one, these constraints can be slightly relaxed and jointly enforced by requiring the product of the ratios $C_\rho=S_\rho/\rho_{\mathrm{ap}}$ and $C_z=S_z/z_{\mathrm{dof}}$ be less than 1:

$$C_{z,\rho}=C_zC_\rho<1 \qquad (6)$$

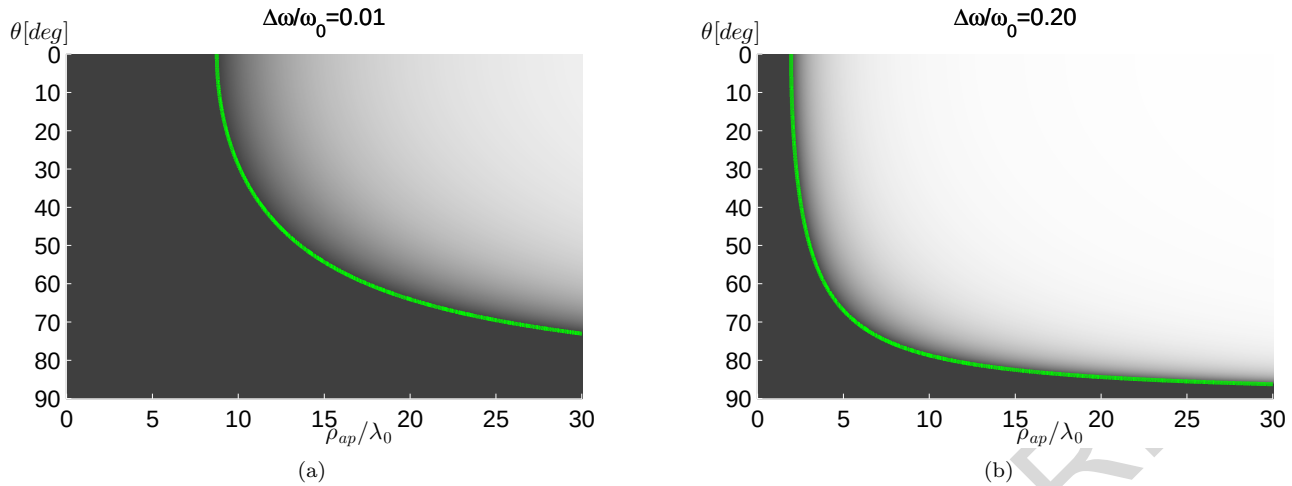

FIG. 1. The green hyperbola represents the boundary between the region of efficient (in white) and non-efficient confinement (in grey) for ideal UXWs, when fractional bandwidths of (a) $\overline{\Delta\omega} = 0.01$ and (b) $\overline{\Delta\omega} = 0.2$ are considered. The region of efficient confinement increases for larger bandwidths. In any case, this region corresponds to electrically large apertures with small axicon angles.

where $C_{z,\rho}$ gives a measure of the spatial and temporal confinement for a practical realization of a generic X-wave. The smaller is $C_{z,\rho}$ the more confined is the X-wave. Obviously, for $C_{z,\rho} = 1$ there is no efficient confinement, since the transverse or the longitudinal spot widths exceed the aperture size or the depth of field, respectively.

In the following, both the transverse and the longitudinal profiles of the ideal X-wave are calculated in closed forms assuming *uniform frequency spectra*. The analysis allows for the evaluation of C_ρ and C_z, thus the spatiotemporal confinement properties of ideal X-waves. Finally, it is worth mentioning that the previous discussion on the confinement capabilities of X-waves is not related to any assumption on the chosen frequency spectrum.

III. ANALYTICAL DESCRIPTION OF IDEAL AND DISPERSIVE X-WAVES WEIGHTED WITH A UNIFORM SPECTRUM

In this section, we consider a bandpass frequency spectrum centered around a carrier angular frequency ω_0 and zero outside a certain frequency band $\Delta\omega$:

$$F(\omega) = \begin{cases} 1 & |\omega - \omega_0| \leq \Delta\omega/2 \\ 0 & \text{elsewhere} \end{cases} \tag{7}$$

This assumption agrees with the physical realizability [37] of any electromagnetic device that may generate nondiffractive Bessel beams only over a well-defined frequency range. In the following, such band-limited X-waves are called uniform frequency-spectrum X-waves (UXWs). It is worth mentioning that theoretical works concerning this subclass of X-waves, as well as different choices of frequency spectra, have been widely investigated in [38] by means of the bidirectional decomposition technique (see [39]).

A. Ideal Uniform X-Waves

By assuming the spectrum in (7), the integral in Eq. (4) for a UXW reduces to:

$$\chi^{\mathrm{U}}(\rho, z, t) = \int_{\omega_0 - \Delta\omega/2}^{\omega_0 + \Delta\omega/2} J_0\left(\frac{\omega}{c}\sin\theta\rho\right) \times \exp\left[-j\frac{\omega}{c}\cos\theta\left(z - \frac{ct}{\cos\theta}\right)\right] d\omega \tag{8}$$

The spatial confinement properties of an X-wave weighted with a uniform spectrum can be easily determined by calculating the integral in Eq. (8) along both the z- and ρ-axis. Note that, since the UXW is assumed to be a superposition of ideal Bessel beams, their nondiffractive and nondispersive behavior implies the rigid transport of the pulse. As a consequence, the transverse ($\chi_{\mathrm{t}}^{\mathrm{U}}(\rho, t)$) and longitudinal ($\chi_{\mathrm{l}}^{\mathrm{U}}(z, t)$) profiles of the UXWs depend on the single variable $z - ct/\cos\theta$ (for the sake of simplicity we assume $t = 0$.)

In particular, the transverse amplitude profile of a UXW is given by:

$$\chi_{\mathrm{t}}^{\mathrm{U}}(\rho) = |\chi(\rho, z = 0, t = 0)| = \left| \int_{\omega_{\mathrm{m}}}^{\omega_{\mathrm{M}}} J_0\left(\frac{\omega}{c}\sin\theta\rho\right) d\omega \right| = \left| \frac{xc}{2\rho\sin\theta} [\pi \mathbf{H}_0(x) J_1(x) + (2 - \pi \mathbf{H}_1(x)) J_0(x)]_{x_{\mathrm{m}}}^{x_{\mathrm{M}}} \right| \tag{9}$$

where $\mathbf{H}_0(\cdot)$ and $\mathbf{H}_1(\cdot)$ are the Struve functions of zero and first order [40], respectively, and where

$$\omega_{\mathrm{M}} = \omega_0 + \Delta\omega/2 \qquad \omega_{\mathrm{m}} = \omega_0 - \Delta\omega/2 \tag{10}$$

$$x_{\mathrm{M}} = \frac{\omega_{\mathrm{M}}\rho\sin\theta}{c} \qquad x_{\mathrm{m}} = \frac{\omega_{\mathrm{m}}\rho\sin\theta}{c} \tag{11}$$

It can be shown that the expression in Eq. (9) is very well approximated by:

$$\chi_{\mathrm{t}}^{\mathrm{U}}(\rho) \simeq \Delta\omega \left| J_0\left(\frac{\omega_0\sin\theta\rho}{c}\right)\right| \tag{12}$$

for small arguments of $J_0(\cdot)$. Note that Eq. (12) simply represents the product of the integrand function in Eq. (9) evaluated at the carrier frequency and the bandwidth, hence Eq. (12) can be interpreted as a result of the Mean Value Theorem [41].

Similarly, the longitudinal amplitude profile of a UXW is given by:

$$\chi_{\mathrm{l}}^{\mathrm{U}}(z) = |\chi(\rho=0,z,t=0)| = \left|\int_{\omega_{\mathrm{m}}}^{\omega_{\mathrm{M}}} \exp\left(-j\frac{z\omega}{c}\cos\theta\right) d\omega\right| \tag{13}$$

The integration over ω yields:

$$\chi_{\mathrm{l}}^{\mathrm{U}}(z) = \Delta\omega \left|\mathrm{sinc}\left(\frac{z\Delta\omega\cos\theta}{2c}\right)\right| \tag{14}$$

From Eqs. (12) and (14) it is possible to evaluate the spot size of the UXW. Here, we consider as spot size the null-to-null distance of the amplitude profile over both axes. The quantities S_ρ and S_z previously defined are then given by:

$$S_\rho = \frac{2j_{0,1}c}{\omega_0\sin\theta} \tag{15}$$

$$S_z = \frac{4\pi c}{\Delta\omega\cos\theta} \tag{16}$$

where $j_{0,1} = 2.4048$ identifies the first null of the J_0 function. As stated in Section II, an efficient spatial confinement takes place only when the constraint in Eq. (6) is respected.

Thus, using Eqs. (15), and (16) in Eq. (6), and expressing the aperture size ρ_{ap} in terms of the operating wavelength $\lambda_0 = 2\pi c/\omega_0$, yields:

$$C_{z,\rho}^{\mathrm{U}} = \underbrace{\frac{j_{0,1}}{\pi m\sin\theta}}_{C_\rho}\underbrace{\frac{2\sin\theta}{m\overline{\Delta\omega}\cos^2\theta}}_{C_z} = \frac{j_{0,1}}{\pi m^2\cos^2\theta\overline{\Delta\omega}} < 1 \tag{17}$$

where $m = \rho_{\mathrm{ap}}/\lambda_0$ is the aperture radius in number of wavelenghts and $\overline{\Delta\omega} = \Delta\omega/\omega_0$ is the fractional bandwidth. Note that in Eq. (17) a ratio with respect to the aperture size has been considered, even if the fields are here computed by neglecting the finiteness of the aperture. However, Eq. (17) will allow for evaluating the impact of different parameters on the shape of the wave. This information will be useful even in the practical case of a finite aperture, discussed in Section IV.

In Fig. 1, the green hyperbola delimits a region of θ, m values for which Eq. (17) is satisfied, for two different values of the fractional bandwidth: $\overline{\Delta\omega} = 0.01$ (Fig. 1a) and $\overline{\Delta\omega} = 0.2$ (Fig. 1b). As clearly shown, the region of efficient confinement increases as the fractional bandwidth increases up to $\overline{\Delta\omega} = 0.2$. Note that for higher values of $\overline{\Delta\omega}$ there are no significant changes with respect to Fig. 1b.

However, from Fig. 1 it is easy to infer that electrically large apertures (high m) and low axicon angles θ are required to efficiently confine a pulse, even for an ideal UXW. Furthermore, it is clear from Eq. (17) that the fractional bandwidth $\overline{\Delta\omega}$ controls the pulse confinement along the z-axis (C_z) without affecting the confinement along the ρ-axis (C_ρ). Conversely, θ affects both C_ρ and C_z. In particular, as θ increases, the pulse is more confined along ρ but spreads along z, and viceversa.

In the following, Eq. (17) will be considered as an upper-bound limit for the confinement factor of both dispersive and dispersive-finite UXWs based on the ideal assumptions used for its derivation.

B. Dispersive Uniform X-Waves

In the previous subsection we assumed that the *axicon angle* is the same for each frequency within the considered band, and thus both the longitudinal and transverse wavenumbers, given by $k_\rho = (\omega/c)\sin\theta$ and $k_z = (\omega/c)\cos\theta$, respectively, are also linear functions of frequency, as required for generating ideal localized waves [1, 2, 38]. However, in most electromagnetic devices, especially for those with considerable fractional bandwidths, a non-linear relationship between k_z, k_ρ and ω is usually assumed, thus dispersion cannot be neglected [12, 14, 42].

Generally, the dependence of both longitudinal and transverse wavenumbers on ω is not known in closed-form, but, for most cases (especially for narrow-band signals), it can be accurately described by the first terms of a Taylor series expansion [43]. As a consequence, the mathematical description of a dispersive UXW is approximated by

$$\begin{aligned}\chi^{\mathrm{U}}(\rho,z,t) &= \int_{\omega_m}^{\omega_M} J_0\left[k_\rho(\omega)\rho\right]\exp\left[-jk_z(\omega)z\right]\exp\left(j\omega t\right)d\omega \\ &\simeq \int_{-\Delta\omega/2}^{\Delta\omega/2} J_0\left[\left(k_{\rho0}k_{\rho1}\omega' + \frac{1}{2}k_{\rho2}\omega'^2\right)\rho\right] \\ &\quad\times\exp\left\{-j\left[\left(k_{z0}+k_{z1}\omega'+\frac{1}{2}k_{z2}\omega'^2\right)z\right]\right\} \\ &\quad\times\exp\left[j(\omega'+\omega_0)t\right]d\omega'\end{aligned} \tag{18}$$

where $\omega' = \omega - \omega_0$, whereas $k_{\rho 0}, k_{\rho 1}$, $k_{\rho 2}$ and k_{z0}, k_{z1}, k_{z2} represent the coefficients of the second-order approximation for the transverse wavenumber k_ρ and for the longitudinal wavenumber k_z, respectively. Note that, k_{z0}, k_{z1}, k_{z2} can be related to $k_{\rho 0}, k_{\rho 1}$, $k_{\rho 2}$ by using the second-order approximations for k_ρ and k_z in Eq. (2). After some algebra, one gets the sought relations

$$k_{z0} = \sqrt{k_0^2 - k_{\rho 0}^2} \tag{19a}$$

$$k_{z1} = (k_0 c^{-1} - k_{\rho 0} k_{\rho 1})/k_{z0} \tag{19b}$$

$$k_{z2} = (c^{-2} - k_{\rho 1}^2 - k_{\rho 0} k_{\rho 2} - k_{z1}^2)/k_{z0} \tag{19c}$$

where $k_0 = \omega_0/c$. Furthermore, k_{z0} and k_{z1} are related to the phase velocity and group velocity, respectively, whereas k_{z2} accounts for the Group Velocity Dispersion (GVD) (an exhaustive analysis on this can be found in [32]).

As a difference with respect to Eq. (8), the transport of the pulse is no longer rigid, hence both the transverse and longitudinal profiles depend on time. Moreover, the transverse profile $\chi_{\rm t}^{\rm U}(\rho, t)$, as a function of time, can only be calculated numerically. Nevertheless, $\chi_{\rm t}^{\rm U}(\rho, t=0)$ is still well approximated by Eq. (8) provided that θ is now calculated at ω_0

$$\begin{aligned}\chi_{\rm t}^{\rm U}(\rho, t=0) &\simeq \Delta\omega \left| J_0\left(k_{\rho 0}\rho\right)\right| \\ &= \Delta\omega \left| J_0\left(\frac{\omega_0 \sin\theta_0 \rho}{c}\right)\right| \end{aligned} \tag{20}$$

where $\theta_0 = \arcsin[k_\rho(\omega_0)/k(\omega_0)]$ is the axicon angle at the carrier frequency. Note that, for sufficiently low values of $k_{\rho 1}$, Eq. (20) is a good approximation even for $t > 0$.

For the longitudinal amplitude profile, an analytical closed-form expression still exists and is given by

$$\begin{aligned}\chi_{\rm l}^{\rm U}(z,t) \simeq &\left| \mathrm{erf}\left[\sqrt{\frac{jzk_{z2}}{2}}\left(\omega' + \frac{zk_{z1} - t}{zk_{z2}}\right)\right]_{\omega'=-\Delta\omega/2}^{\omega'=\Delta\omega/2}\right| \\ &\times \left|\sqrt{\frac{\pi}{j2k_{z2}z}}\right| \end{aligned} \tag{21}$$

where $\mathrm{erf}(\cdot)$ is the error function [40]. Note that, $k_{z2} = 0$ (i.e., when a first-order Taylor series expansion of k_z is assumed) is a removable singularity. Thus, as long as $k_{z2} \to 0$, Eq. (21) reduces to Eq. (14). It is possible to evaluate the spot size of a dispersive UXW in an approximated analytical form for Eq. (20) or numerical form for Eq. (21). However, both the transverse and longitudinal spot widths are upper-bounded by Eqs. (15) and (16), thus Eq. (17) and its related Fig.1 can still be used as references. In particular, for narrow bandwidths, the spot widths of a dispersive X-wave coincide with those of an ideal X-wave, and thus Fig. 1(a) is still an accurate description. For wider bandwidths, the transverse spot width remains unchanged with respect to the ideal case (as clear by comparing Eqs. (20) and (12)), whereas the longitudinal spot size can only be calculated numerically and it is generally greater than the ideal one. As a consequence, Fig.1(b) should yield an underestimation of the pulse longitudinal size.

In the following Sections IV and V, numerical results for a dispersive-finite X-wave, i.e., taking into account both the dispersion and the finiteness of the radiating aperture, are shown considering a defined aperture field distribution. In particular, Section IV describes the physical device considered for the generation of X-waves, whereas Section V highlights the effect of the bandwidth on the focusing properties of the generated pulse.

IV. FINITE AND DISPERSIVE X-WAVES

It has been recently shown [15] that Bessel beams can be efficiently generated through an inward traveling wave aperture distribution. As a main difference with respect to other realizations [14], [44], inward aperture field distribution generates nondiffractive Bessel-like beams over a wide fractional bandwidth. Therefore, in order to introduce the effect of the finiteness of the radiating structure, we will calculate the electric field $E^{\rm rad}$ radiated by such a distribution over a finite aperture plane. The UXW is then generated by taking the integral

$$\chi(\rho, z, t) = \int_{\omega_{\rm m}}^{\omega_{\rm M}} E^{\rm rad}(\rho, z) \exp(j\omega t) d\omega \tag{22}$$

that is the general form of Eq. (8) where $E^{\rm rad}$ replaces the ideal Bessel beam distribution. Note that $E^{\rm rad}$ is here considered as a proper scalar component of the total radiated electric field $\mathbf{E}^{\rm rad}$ which can be calculated e.g., as [43, 45]:

$$\mathbf{E}^{\rm rad}(\mathbf{r}) = \frac{1}{4\pi}\int_{S'} (\mathbf{r} - \mathbf{r}') \times \mathbf{E}_t(\mathbf{r}') \frac{(1 + jkR)}{R^3} e^{-jkR} dS' \tag{23}$$

where $\mathbf{r}$, and $\mathbf{r}'$ are the observation and source points, respectively, $R = |\mathbf{r} - \mathbf{r}'|$ is the euclidean distance between the observation and source points, S' is the surface on which the electromagnetic sources are localized, and $\mathbf{E}_t = \hat{\mathbf{n}} \times \mathbf{E} \times \hat{\mathbf{n}}$ is the tangential electric field component ($\hat{\mathbf{n}}$ being the unit vector normal to the surface).

According to [15], an inward cylindrical traveling wave aperture distribution is able to generate a Bessel beam. The aperture distribution of the tangential electric field is assumed equal to a first-kind, zeroth-order Hankel aperture distribution $\mathbf{E}(\rho, \phi) = H_0^{(1)}(k_\rho(\omega_0)\rho)\hat{\mathbf{p}}_0$ where $\hat{\mathbf{p}}_0$ is an arbitrary polarization vector, and $k_\rho(\omega_0)$ is fixed a priori. In this work, a circular polarization has been assumed. The structure synthesizing such aperture field distribution is shown in Fig. 2(a). It consists of a dielectric filled radial waveguide loaded with radiating slots operating at $f_0 = 60\,\mathrm{GHz}$ and with a finite radius of $\rho_{\rm ap} = 15\lambda_0 = 75\,\mathrm{mm}$, centrally fed by a coaxial probe. The aperture field distribution has an approximate dis-

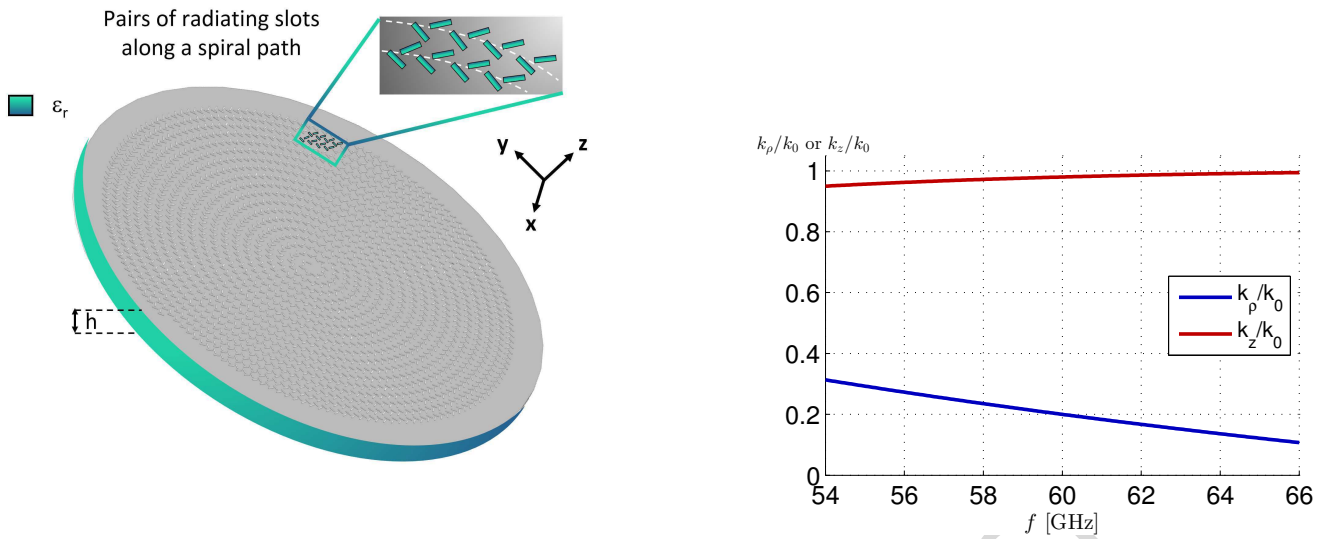

(a) (b)

FIG. 2. (a) Axonometric representation of the dielectric filled radial waveguide loaded with radiating slots. The device is centrally fed by a coaxial probe. (b) Dispersion of the longitudinal (red line) and transverse normalized wavenumbers (blue line) with respect to the frequency in a fractional bandwidth $\overline{\Delta\omega} = 0.2$ around the carrier frequency $f_0 = 60\,\mathrm{GHz}$ for the structure in Fig. 2a.

persion behavior described by the expansion:

$$k_\rho(\omega) = k_\rho(\omega_0) - \frac{\sqrt{\varepsilon_r}}{c}(\omega - \omega_0) \tag{24}$$

where $\varepsilon_r = 1.04$ is the relative permittivity of the dielectric material filling the radial waveguide. Such peculiar dispersion relation follows from the spiral alignment of the radiating slots that is needed to synthesize the desired aperture distribution. It is worth here noting that such wavenumber dispersion defines a space harmonic of backward type [46] as required to radiate well-collimated focus wave modes [47]. As shown in Fig. 2(b), the transverse wavenumber normalized with respect to k ($\hat{k}_\rho = k_\rho/k$) at f_0 is $\hat{k}_\rho(\omega_0) = 0.2$, and thus the operating axicon angle is $\theta_0 \simeq 11°$ with a depth of field at f_0 equal to $z^{(c)}_{\mathrm{dof}} \simeq 367\,\mathrm{mm}$. It is worth mentioning that the design parameters of the proposed structure have been shown according to the results in Fig. 1 requiring an axicon angle smaller than 50° for a radiating aperture of $15\lambda_0$. The integral in Eq. (22) is then computed by using Eq. (23).

In the following section, the effect of the bandwidth on the spatial properties of the pulse is highlighted by showing different UXW generations for various values of the fractional bandwidth, considering the ideal case (Sec. III A), the dispersive case (Sec. III B) and this dispersive-finite case (Sec. IV).

V. RESULTS AND DISCUSSION

Fig. 3 shows the 2D maps of the normalized intensity (defined as $|\chi^{\mathrm{U}}(\rho, z, t)|^2$) of the pulse for the ideal (see Fig. 3(a)-(d)), the dispersive (see Fig. 3(e)-(h)), and the dispersive-finite (see Fig. 3(i)-(l)) cases, for a fractional bandwidth of $\overline{\Delta\omega} = 0.05$ (see Fig. 3(a), (e), (i)), $\overline{\Delta\omega} = 0.1$ (see Fig. 3(b), (f), (j)), $\overline{\Delta\omega} = 0.15$ (see Fig. 3(c), (g), (k)), $\overline{\Delta\omega} = 0.2$ (see Fig. 3(d), (h), (l)). The field intensities are shown on a ρz-plane limited on the ρ-axis by the aperture of the finite structure ($\rho_{\mathrm{ap}} = 15\lambda_0$, $\lambda_0 = 5$ mm) and on the z-axis by the depth of field achieved at the carrier frequency $z^{(c)}_{\mathrm{dof}} = 367$ mm. Here it is worth to remark that the depth of field is generally a function of the frequency (as clear from Eqs. (3), (5), and (24)) and thus its value varies within the bandwidth in both the dispersive and the finite case. Conversely, in the ideal case, the pulse is assumed to be nondispersive and nondiffractive, thus the depth of field is constant over all the frequency range. In the ideal case we have assumed $\hat{k}_\rho(\omega) = \hat{k}_\rho(\omega_0)$ and thus $\theta(\omega) = \theta_0$.

As shown in Fig. 3, the pulse is depicted at a fixed time frame when its maximum has reached the distance $z_{\mathrm{p}} = z^{(c)}_{\mathrm{dof}}/2 \simeq 183$ mm (the time evolution of the pulse is available as Multimedia view in .mp4 format). For the ideal case (see first row of Fig. 3), the previous distance is reached for an instant of time $t_{\mathrm{p}} < z_{\mathrm{p}}/c$ ($t_{\mathrm{p}} = 0.60$ ns, $z_{\mathrm{p}}/c = 0.61$ ns), which means that the pulse is propagating superluminally, as expected for a nondispersive pulse whose phase velocity is greater than c. On the other hand, in both the dispersive and dispersive-finite case $t_{\mathrm{p}} > z_{\mathrm{p}}/c$ ($t_{\mathrm{p}} = 0.73$ ns) and hence the pulse is obviously subluminal due to dispersion.

Figs. 3(a)-(d) clearly show the impact of the bandwidth in the z-confinement of the pulse: the greater is the fractional bandwidth, the narrower is the spot size along the z axis. This behavior is also observable in Fig. 3(e)-(h) and Fig. 3(i)-(l), where the longitudinal spot size S_z

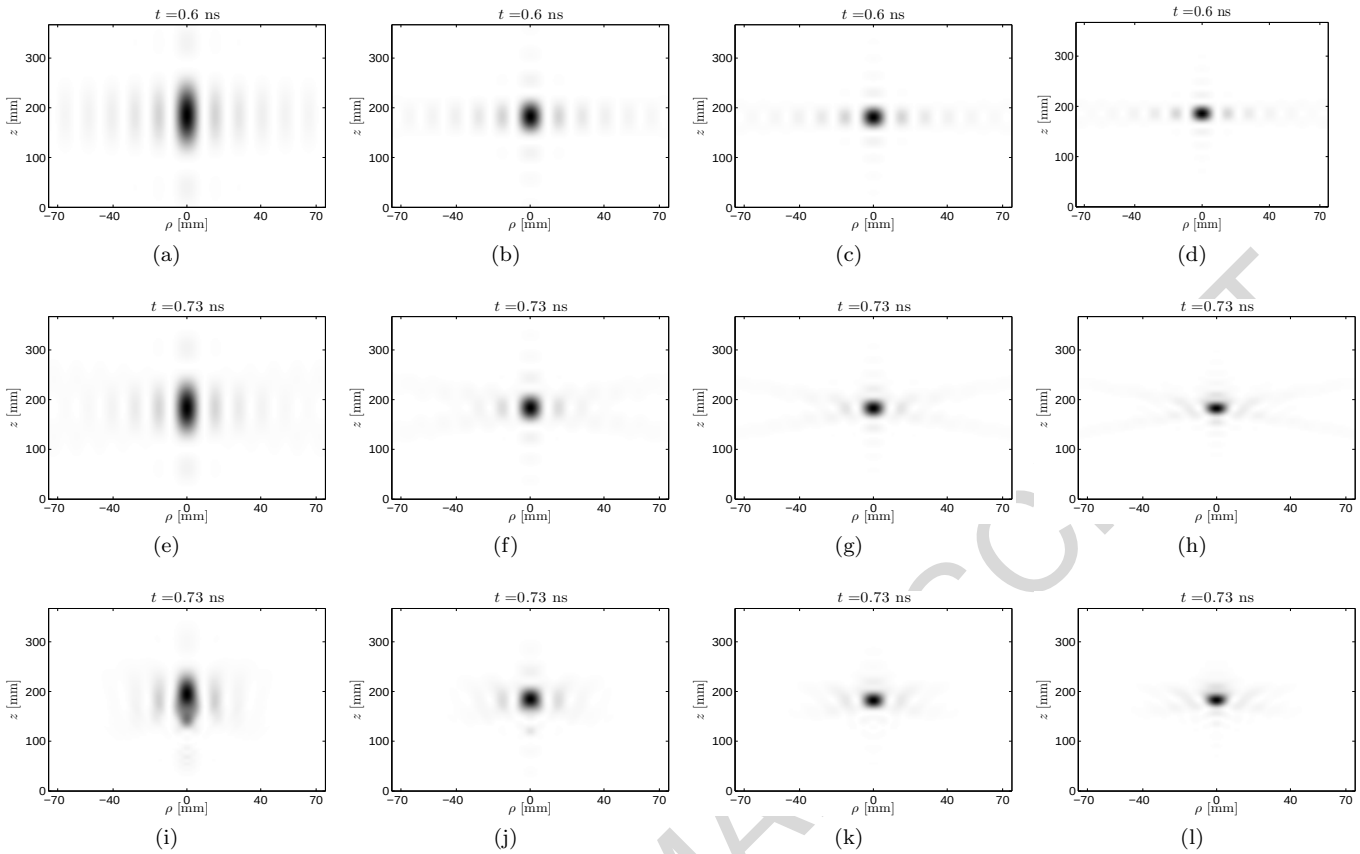

FIG. 3. 2D normalized intensities for ideal (first row: (a)-(d)), dispersive (second row: (e)-(h)), and dispersive-finite (third row: (i)-(l)) UXWs, when the pulse has reached half the propagating distance of $z_{\mathrm{dof}}^{(c)}$. The numerical results are shown for $\overline{\Delta\omega} = 0.05$ (first column: (a), (e), (i)), $\overline{\Delta\omega} = 0.1$ (second column: (b), (f), (j)), $\overline{\Delta\omega} = 0.15$ (third column: (c), (g), (k)), and $\overline{\Delta\omega} = 0.2$ (fourth column: (d), (h), (l)). See Multimedia view Vid-3d, Vid-3h, and Vid-3l for the whole time evolution of the pulse for cases (d), (h), and (l), respectively.

of the pulse decreases as the bandwidth increases. However, in these last two cases the pulse no longer retains its shape as it propagates, hence both the transverse and the longitudinal profiles of the pulse are different at each time frame. In particular, for both dispersive and dispersive-finite cases, the spot size over both ρ and z directions increases with time.

This effect is highlighted in Fig. 4(a)-(f) where the time evolution of both the transverse (Fig. 4(a)-(c)) and the longitudinal (Fig. 4(d)-(f)) profiles of ideal (Fig. 4(a), (d)), dispersive (Fig. 4(b), (e)), and dispersive-finite (Fig. 4(c), (f)) UXWs with a fractional bandwidth $\overline{\Delta\omega} = 0.2$ are shown for three different instants of time t_i such that the pulse traveled for a distance $z_i = iz_{\mathrm{dof}}^{(\mathrm{c})}/2$, $i = 1, 2, 3$. As expected, the transverse profile of an ideal UXW does not depend on time, whereas for dispersive and dispersive-finite UXWs it is strongly time-dependent. In particular, as time increases the maximum intensity is abruptly attenuated and simultaneously the transverse spot size is considerably widened for energy conservation. On the other hand, the longitudinal profile of an ideal UXW is rigidly transported over the z axis (Fig. 4(d)), whereas for the dispersive and dispersive-finite UXWs the transport is no longer rigid due to dispersion (Figs. 4(e), (f)). More properly, from Figs. 4(e), and (f), it is clear that both the amplitude reduction and longitudinal spot size enlargement of the main spot cause a non-negligible pulse distortion.

The whole time evolution of both spatial confinement properties of the considered UXWs are differently represented in Fig. 5(a) and in Fig. 5(b), along the transverse and the longitudinal direction, respectively. The half power beamwidth (HPBW) is calculated with respect to the absolute maximum at each time frame. Figs. 5(a) and (b) show the evolution of the spot size with respect to time only for a fractional bandwidth $\overline{\Delta\omega} = 0.2$, for which the effects of the dispersion and of the truncation are more pronounced.

In details, in Fig. 5(a) it can be noticed that the transverse profile of the dispersive-finite UXW starts spreading at the time frame when the pulse has reached the minimum depth of field $z_{\mathrm{dof}}^{(\mathrm{min})}$ of the constituent waves. Slightly after, the transverse spreading increases almost linearly with time. As expected, the ideal UXW

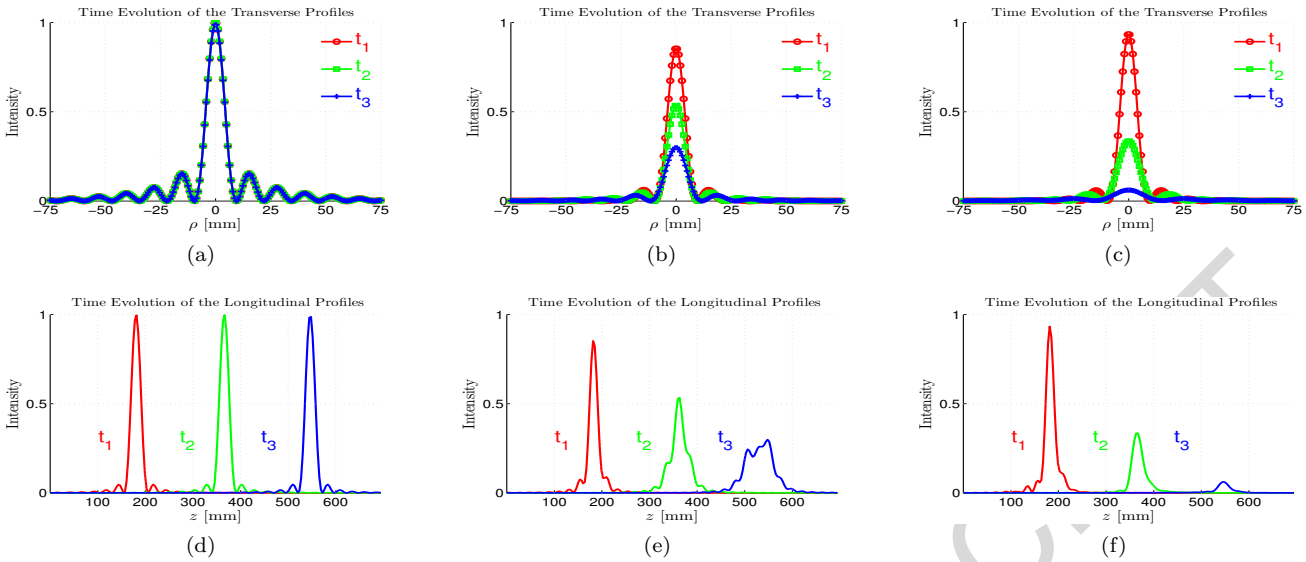

FIG. 4. Transverse (a)-(c) and longitudinal (d)-(f) profiles normalized at the absolute maximum with respect to time for (a), (d) ideal, (b), (e) dispersive, (c), (f) dispersive-finite UXWs with a fractional bandwidth $\overline{\Delta\omega} = 0.2$ at timestamps t_1, t_2 and t_3 corresponding to the time instants when the pulse has reached the distances of $z_1 = 0.5z_{\rm dof}^{\rm (c)}$, $z_2 = z_{\rm dof}^{\rm (c)}$, and $z_3 = 1.5z_{\rm dof}^{\rm (c)}$.

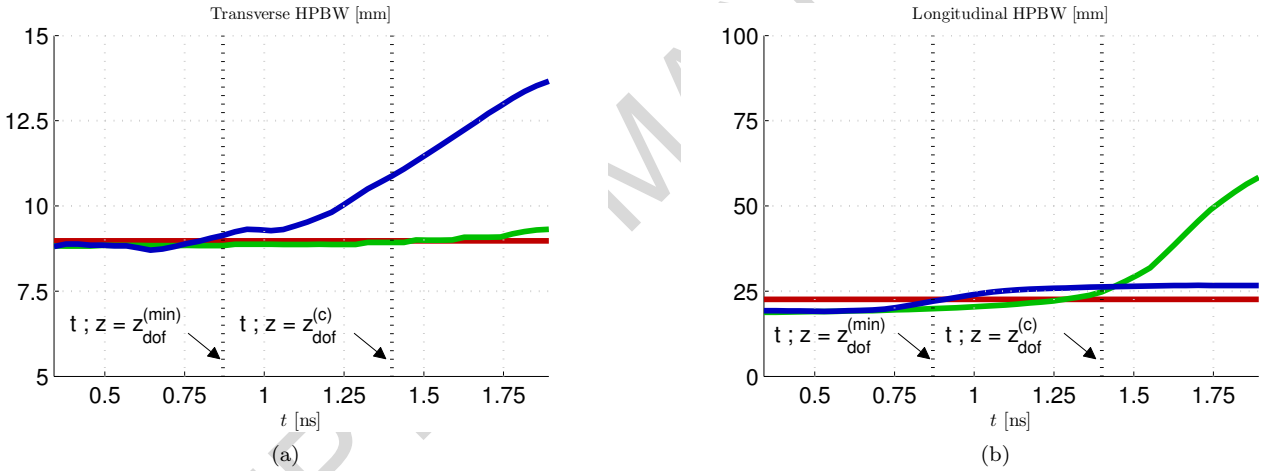

FIG. 5. Evolution of the (a) transverse and (b) longitudinal spot size (HPBW) vs. t. The ideal (red line), dispersive (green line), and the dispersive-finite case (blue line) are represented for $\overline{\Delta\omega} = 0.2$.

maintains a constant transverse profile for all the time, whereas the dispersive UXW has a negligible spreading (less than 2 mm here) only at the end of the considered time propagation.

In Fig. 5(b) a different behavior is observable. As expected, the ideal UXW retains its longitudinal spot size as it propagates, whereas the dispersive UXW spreads along the longitudinal axis after a certain distance at which the spot size increases almost linearly with time. However, the dispersive-finite UXW only slightly spreads over the longitudinal direction. Such a different behavior for the transverse and the longitudinal spreading is also visible in Figs. 4(e) and (f), and can be interpreted in terms of diffraction and dispersion phenomena. In general, an attenuation of the field intensity requires a beam spreading (either transverse or longitudinal) to grant energy conservation. Now, in dispersive-finite UXWs, the Bessel beam profiles are no longer transversely confined after the depth of field (Fig. 4(c)), as expected for their finite aperture realizations [3]. This means that the attenuation of the field intensity does not necessarily correspond to a longitudinal spreading (Fig. 4(f)), since a transverse spreading is already present. On the other hand, in a dispersive UXW, no significant transverse spreading is observed (Fig. 4(b)), so that the attenuation of the field intensity should correspond to a longitudinal

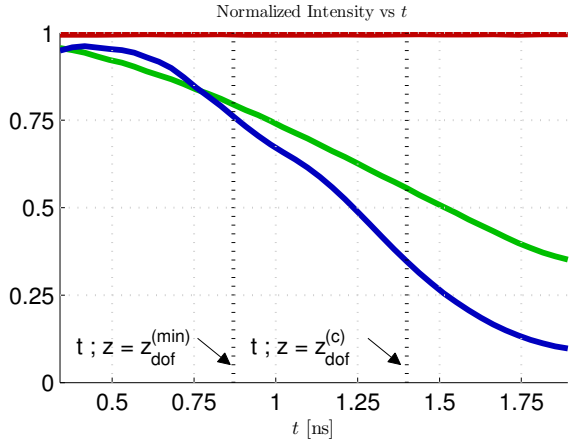

FIG. 6. Evolution of the normalized intensity vs. time t. The ideal (red line), dispersive (green line), and the dispersive-finite case (blue line) are represented for $\overline{\Delta\omega} = 0.2$.

spreading (Fig. 4(e)).

Finally, in Fig. 6 the time evolution of the normalized intensities of ideal, dispersive, and dispersive-finite UXWs have been calculated for $\overline{\Delta\omega} = 0.2$. It is clear that the ideal UXW is a soliton-like solution in the sense that its normalized intensity is kept constant for all times. On the other hand, the normalized intensities of dispersive and dispersive-finite UXWs decrease with time as the pulse propagates. In the dispersive case, the attenuation is due to the different velocities of the various components of the pulse and thus the intensity fades out even if the pulse is fed with infinite energy. In the dispersive-finite case, the intensity is slightly attenuated (less than 25%) until the pulse reaches the $z_{\rm dof}^{(\rm min)}$. After that distance the intensity decreases rapidly and then vanishes for a sufficiently long time (or propagating distance), as required for any physical system which is fed with finite energy. It is worth noting that the strong fading of the pulse after the depth of field $z_{\rm dof}$ strengthens our initial assumption to define a metric over the z-axis with respect to the depth of field of a general X-wave.

VI. CONCLUSION

We have analyzed both the spatial and the temporal properties of ideal and dispersive X-waves generated by a finite radiating aperture in the presence of dispersion. In particular, we have first defined an efficiency of confinement for ideal X-waves, i.e., nondiffractive waves generated as the superposition of ideal Bessel beams. This analysis revealed that, even in the ideal case, some limitations exist to produce pulses that are efficiently confined along both the transverse and longitudinal axes. In particular, large fractional bandwidths (up to 20%) and electrically large apertures with low-axicon angles of the constituent Bessel beams are required. Moreover, we provided exact and approximated analytically closed-form relations for the calculation of the transverse and longitudinal profiles for both ideal and dispersive X-waves with a limited uniform spectrum.

On this ground, the propagation of ideal, dispersive, and dispersive-finite X-waves has been considered and then compared for different values of the fractional bandwidth of the relevant spectra. Numerical results have shown that the longitudinal spot size always decreases as the bandwidth increases. Furthermore, for a dispersive-finite X-wave, both the transverse and longitudinal spot size spread as the pulse travels beyond the minimum depth of field achieved at the minimum frequency of the spectrum. For a dispersive-finite X-wave the maximum intensity of the pulse reduces as it propagates beyond the nondiffractive range of the constituent waves. Nevertheless, when a dispersive-finite X-wave propagates within the minimum depth of field associated to the considered spectra, its spatiotemporal properties coincide with those of an ideal X-wave, therefore its spot size and its intensity are almost constant as it propagates. In the dispersive-finite case considered here at millimeter wavelengths, we have demonstrated that a radiating aperture of radius 7.5 cm fed by a 60-GHz signal with uniform spectrum over a 20% fractional bandwidth around the carrier frequency is able to produce X-waves with an almost constant longitudinal spotsize of about 1 cm and a transverse spotsize of about 2.5 cm over a propagating distance of 20 cm.

Further works will be devoted to the study of the confinement of X-waves by full-wave simulations and measurements.

[1] H. E. Hernández-Figueroa, M. Zamboni-Rached, and E. Recami, *Nondiffracting Waves* (John Wiley & Sons, 2013).
[2] H. E. Hernández-Figueroa, M. Zamboni-Rached, and E. Recami, *Localized Waves*, Vol. 194 (John Wiley & Sons, 2007).
[3] J. Durnin, J. Opt. Soc. Am. A **4**, 651 (1987).
[4] J. Durnin, J. J. Miceli Jr., and J. H. Eberly, Phys. Rev. Lett. **58**, 1499 (1987).
[5] R. Herman and T. Wiggins, J. Opt. Soc. Am. A **8**, 932 (1991).
[6] J. Arlt and K. Dholakia, Opt. Commun. **177**, 297 (2000).
[7] S. Monk, J. Arlt, D. Robertson, J. Courtial, and M. Padgett, Opt. Commun. **170**, 213 (1999).

[8] G. Milne, G. D. Jeffries, and D. T. Chiu, Appl. Phys. Lett. **92**, 261101 (2008).
[9] W. Williams and J. Pendry, J. Opt. Soc. Am. A **22**, 992 (2005).
[10] A. Vasara, J. Turunen, and A. T. Friberg, J. Opt. Soc. Am. A **6**, 1748 (1989).
[11] P. Lemaitre-Auger, S. Abielmona, and C. Caloz, IEEE Trans. Antennas Propag. **61**, 1838 (2013).
[12] A. Mazzinghi, M. Balma, D. Devona, G. Guarnieri, G. Mauriello, M. Albani, and A. Freni, IEEE Trans. Antennas Propag. **62**, 3911 (2014).
[13] M. F. Imani and A. Grbic, IEEE Trans. Antennas Propag. **60**, 3155 (2012).
[14] M. Ettorre, S. M. Rudolph, and A. Grbic, IEEE Trans. Antennas Propag. **60**, 2645 (2012).
[15] M. Albani, S. Pavone, M. Casaletti, and M. Ettorre, Opt. Express **22**, 18354 (2014).
[16] M. Zamboni-Rached and E. Recami, arXiv preprint arXiv:1408.5635 (2014).
[17] M. Zamboni-Rached, M. C. de Assis, and L. A. Ambrosio, Appl. Optics **54**, 5949 (2015).
[18] M. Lapointe, Opt. Laser Technol. **24**, 315 (1992).
[19] D. McGloin and K. Dholakia, Contemp. Phys. **46**, 15 (2005).
[20] S. Mishra, Opt. Commun. **85**, 159 (1991).
[21] J. N. Brittingham, J. Appl. Phys. **54**, 1179 (1983).
[22] R. W. Ziolkowski, J. Math. Phys. **26**, 861 (1985).
[23] A. Sezginer, J. Appl. Phys. **57**, 678 (1985).
[24] E. Capelas de Oliveira and W. Rodrigues, Phys. Lett. A **291**, 367 (2001).
[25] J.-Y. Lu and J. F. Greenleaf, IEEE Trans. Ultrason. Ferroelectr. Freq. Control **39**, 19 (1992).
[26] J.-Y. Lu and J. F. Greenleaf, IEEE Trans. Ultrason. Ferroelectr. Freq. Control **39**, 441 (1992).
[27] P. Saari and K. Reivelt, Phys. Rev. Lett. **79**, 4135 (1997).
[28] E. Recami, Physica A **252**, 586 (1998).
[29] W. A. Rodrigues Jr and J.-Y. Lu, Found. Phys. **27**, 435 (1997).
[30] A. A. Chatzipetros, A. M. Shaarawi, I. M. Besieris, and M. A. Abdel-Rahman, J. Acoust. Soc. Am. **103**, 2287 (1998).
[31] R. W. Ziolkowski, I. M. Besieris, and A. M. Shaarawi, J. Opt. Soc. Am. A **10**, 75 (1993).
[32] M. A. Porras, G. Valiulis, and P. Di Trapani, Phys. Rev. E **68**, 016613 (2003).
[33] H. Sonajalg and P. Saari, Opt. Lett. **21**, 1162 (1996).
[34] W. Rodrigues, D. S. Thober, and A. Xavier, Phys. Lett. A **284**, 217 (2001).
[35] E. Capelas de Oliveira, W. Rodrigues, D. Thober, and A. Xavier, Phys. Lett. A **284**, 296 (2001).
[36] E. Capelas de Oliveira and W. Rodriguez, Ann. Phys. (Berlin) **7**, 654 (1998).
[37] D. Mugnai, A. Ranfagni, and R. Ruggeri, Phys. Rev. Lett. **84**, 4830 (2000).
[38] M. Zamboni-Rached, E. Recami, and H. E. Hernández-Figueroa, Eur. Phys. J. D. **21**, 217 (2002).
[39] I. M. Besieris, A. M. Shaarawi, and R. W. Ziolkowski, J. Math. Phys. **30**, 1254 (1989).
[40] M. Abramowitz and I. A. Stegun, *Handbook of Mathematical Functions* (New York: Dover, 1962).
[41] W. Rudin, *Principles of Mathematical Analysis* (New York: McGraw-Hill, 1976).
[42] M. Ettorre, S. Pavone, M. Casaletti, and M. Albani, IEEE Trans. Antennas and Propag. **63**, 2539 (2015).
[43] C. A. Balanis, *Advanced Engineering Electromagnetics*, Vol. 111 (Wiley Online Library, 2012).
[44] S. Chávez-Cerda, J. Mod. Opt. **46**, 923 (1999).
[45] J. D. Jackson and J. D. Jackson, *Classical Electrodynamics*, Vol. 3 (New York: Wiley, 1962).
[46] A. A. Oliner and A. Hessel, IRE Trans. Antennas and Propag. **7**, 201 (1959).
[47] E. Heyman, IEEE Trans. Antennas and Propag. **37**, 1604 (1989).
[48] See supplemental Material at URL (will be inserted by publisher) for further details.